Revista Brasileira de Ensino de Física, vol. 46, e20230370 (2024)
www.scielo.br/rbef
DOI: https://doi.org/10.1590/1806-9126-RBEF-2023-0370

Determination of a CO_2 laser beam profile using a Smartphone camera

Gabriel de Toledo Paula[1], Nicolas Ribeiro[1], Jader de Souza Cabral[2], Carlos Renato Menegatti*[1]

[1]Universidade de São Paulo, Escola de Engenharia de Lorena, 12602-810, Lorena, SP Brasil.
[2]Universidade Federal de Uberlândia, Instituto de Física, 38400-902, Uberlândia, MG, Brasil.

Received on November 30, 2023. Revised on January 10, 2024. Accepted on January 11, 2024.

Lasers find extensive applications across a spectrum from academic research to industrial use. In various instances, understanding the intensity profile of laser light is of paramount importance, specifically how its intensity changes along its propagation path. In this study, we introduce an economical and alternative technique for determining the waist of a Gaussian laser beam, leveraging the capabilities of a Smartphone camera. Our methodology entails directing a CO_2 laser onto a thermochromic liquid crystal sheet for specific exposure duration, resulting in a color pattern that evolves over time. This evolving pattern is captured by a Smartphone camera, and selected frames from the recording are processed and analyzed to quantify the beam's waist, denoted as $w(z)$. Our measurements are compared with those obtained through the traditional knife-edge method, demonstrating a substantial degree of agreement. Furthermore, by interpolating the waists calculated through our approach, we were able to ascertain the beam waist at the focus and the focal point of a converging lens, yielding results consistent with the reference method. Our findings underscore the viability of this approach as a cost-effective alternative for characterizing Gaussian beams, with potential applications in optics, laser technology, and studies related to light propagation.

Keywords: CO_2 laser, beam profile, knife-edge, Smartphone camera.

1. Introduction

Since its invention in the 1960s by Theodore Maiman, the laser has emerged as an increasingly indispensable tool in both academic research and everyday problem-solving applications [1–3]. Its name is an acronym for "Light Amplification by Stimulated Emission of Radiation," and its operational principles were introduced to the world by Albert Einstein in the early 20th century [4, 5, p. 4].

The defining feature of laser light is the stimulated emission of photons within an optical cavity. In other words, laser light does not occur naturally and must be generated under specific conditions determined by the physical system, known as the active medium, the geometry of the optical cavity, and the energy input into the active medium, referred to as the pump energy [6, 7]. As a result, laser light has four unique characteristics: (i) high coherence (both spatial and temporal), ensuring a high level of predictability of the electric field $\vec{E}(\vec{r},t)$; (ii) high directionality, resulting in a minimal beam divergence; (iii) high intensity; and (iv) monochromaticity, characterized by a narrow spectral bandwidth [8, 9].

All these characteristics have rendered laser light highly significant in various applications across different fields of science and engineering. In academia, lasers are employed in research related to quantum optics [10, 11], quantum computing and information [12, 13], atomic and molecular physics [14–16], astronomy and cosmology [17, 18], cellular biophysics and biomedicine [19, 20, p. 5], nanotechnology, and new material development [21, 22], as well as material spectroscopy and characterization [23–28], among others. In industry, lasers find application in high-precision cutting [29, 30], alignment and imaging systems, various sensors [31, 32], and more.

For all these applications, understanding the intensity profile of laser light is crucial, i.e., how its power varies along its propagation path. Through experimental measurements (laser light characterization), it is possible to determine how the intensity changes from the center of the beam to its edge at different positions along the propagation path. The size of the beam at different positions is referred to as the beam waist, and in the focal region, where the beam achieves its maximum convergence, its waist reaches a minimum value. However, these experimental measurements typically require costly equipment, such as profilometers (∼ US$ 10,000.00) that provide high-precision intensity profiles, or a method known as knife-edge, which involves numerous experimental measurements, leading to extended measurement times and posing risks to experimenters, particularly when dealing with high-power lasers [33, 34].

*Correspondence email address: renatomenegatti@usp.br

In this work, we propose an alternative low-cost method for determining the waist of a Gaussian beam using a Smartphone camera (SCM). In this method, a CO_2 laser is directed onto a thermochromic liquid crystal sheet for a specific exposure time, generating a color pattern that evolves over time. This pattern is recorded by a Smartphone camera, and specific frames from this recording are selected, processed, and analyzed in order to measure the beam waist(w). As a reference technique, we use the knife-edge method (KEM) to compare the measured w values. The results obtained by both methods are compared, and good agreement is observed, particularly at distances far from the focal point. By interpolating the waists measured by the SCM we were able to calculate the w (beam waist) at the focus and the focal of a converging lens. These values were the same as those calculated by the KEM, the reference method.

2. Theoretical Concepts

In 1879, James Clerk Maxwell presented a system of equations describing the relationships between electric and magnetic fields. These equations are known as Maxwell's equations. In general, Maxwell's equations for vacuum and in the absence of charges and currents are expressed as follows:

$$\nabla \cdot \vec{E} = 0 \tag{1}$$

$$\nabla \cdot \vec{B} = 0 \tag{2}$$

$$\nabla \times \vec{E} = -\frac{\partial \vec{B}}{\partial t} \tag{3}$$

$$\nabla \times \vec{B} = \mu_0 \varepsilon_0 \frac{\partial \vec{E}}{\partial t} \tag{4}$$

Using appropriate mathematical manipulations, it is possible to derive the differential equation describing the propagation of an electromagnetic field in a vacuum, as presented in, as follows:

$$\nabla^2 \vec{E} - \frac{1}{c^2}\frac{\partial^2 \vec{E}}{\partial t^2} = 0 \tag{5}$$

applying the Laplacian operator in cylindrical coordinates in Eq. (5), it is possible to obtain the equation describing the Gaussian beam:

$$E(r,z) = \frac{E_0 w_0}{w(z)} e^{-r^2/w^2(z)} \cdot e^{-i\left[kz - \eta(z) + \frac{kr^2}{2R(z)}\right]} \tag{6}$$

In this equation, the magnitude of the electric field has a Gaussian shape. This means that as the radial coordinate denoted by r increases, the field exponentially decreases, following a Gaussian pattern. This behavior can be observed in Figure 1, representing the mathematical behavior of the field as the coordinate r increases.

Additionally, in Eq. (6), it is possible to extract the spatial propagation behavior:

$$R(z) = z\left(1 + \left(\frac{z_R}{z}\right)^2\right) \tag{7}$$

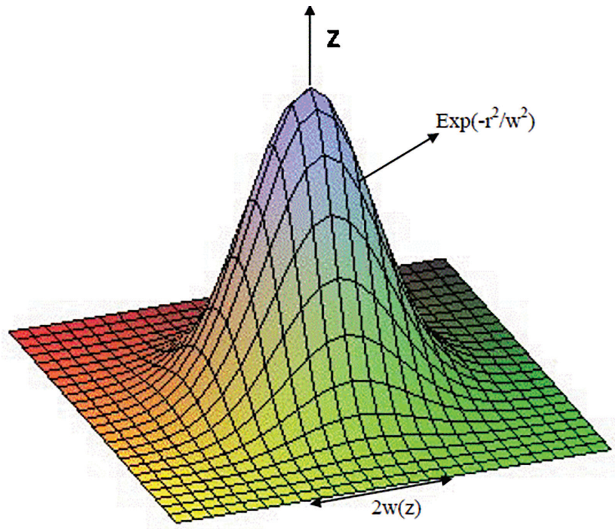

Figure 1: Transverse intensity distribution of the Electric Field.

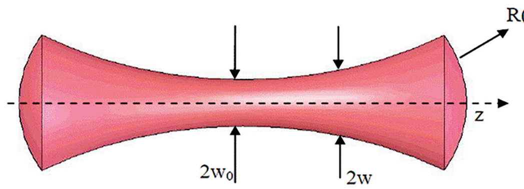

Figure 2: Propagation of a Gaussian beam.

and

$$w(z) = w_0\sqrt{1 + \left(\frac{z - z_c}{z_R}\right)} \tag{8}$$

In Eq. (7), the term $z_R = \pi n w_0^2/\lambda$ is known as the Rayleigh length. In Eq. (8), when $r = w(z)$, the field intensity decreases to 1/e of its value, and at $z = z_c$, $w(z) = w_0$, and this point is known as the beam waist. Figure 2 shows the spatial behavior of the beam.

3. Materials and Methods

3.1. Optical setup

The optical setup (Figure 3) consists of an industrial-class CO_2 laser, model GEM-100, produced by COHERENT, with a power of 130 W, a wavelength of 10.6 μm, and an approximate beam waist of 2.3 mm near the laser output ($\sim$ 20 cm). The beam passed through a set of ZnSe lenses to allow for different waist values. First, the beam passed through a telescope formed by a divergent lens ($F1 = -2$") and a convergent lens ($F2 = 7.5$"), expanding the beam by a factor of 3.8, resulting in awaist of 8.6 mm approximately. Then, the beam was focused by a lens $F3 = 250$ mm and collimated again by another lens $F4 = 250$ mm. Afterward, the beam was incident on the power meter, with its diameter slightly reduced

 DOI: https://doi.org/10.1590/1806-9126-RBEF-2023-0370

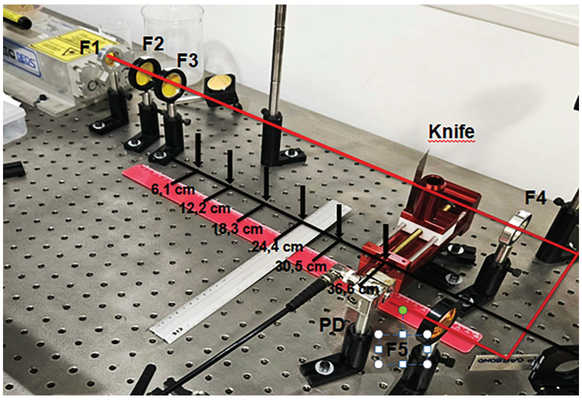

Figure 3: Optical setup.

by a convergent lens $F5 = 100$ mm. A knife, made of a sharp metal piece, was attached to a translator with a precision of 0.05 mm, and this translator was positioned between lenses F3 and F4 to measure the beam at six different positions relative to lens F3.

3.2. Knife-edge method (KEM)

The knife-edge method consists of measuring the power of a beam partially interrupted by a sharp metal piece. Mathematically, this power can be calculated by integrating the radiation intensity $I(r,z) = |E(r,z)|^2$ over the exposed area Eq. (9). In particular, since the knife interrupts the beam by moving in one direction, we need to integrate $I(r,z)$ up to a distance x, as shown in Figure 4, obtaining Eq. (10):

$$P(x) = \int_x^\infty \frac{I_0^2 w_0^2}{w^2(z)} e^{-2(x-x_c)^2/w^2(z)} dx \tag{9}$$

$$P(x) = P_{offset} + P\left\{1 - erf\left[\frac{\sqrt{2}}{w(z)}(x - x_c)\right]\right\} \tag{10}$$

In this equation, P is the total power, x_c is the Gaussian central point, x is the knife position, and $w(z)$ is the beam waist, the quantity we intend to determine.

For power measurements we use a OPHIR broadband thermal sensor, model 30(150)A-BB-18, 30/150 W, air-cooled and aperture of Ø17.5 mm coupled to a power meter model NOVA, total equipment cost about US$ 7,000.00. Figure 5 presents a measurement made by the KEM. The black points represent the measured

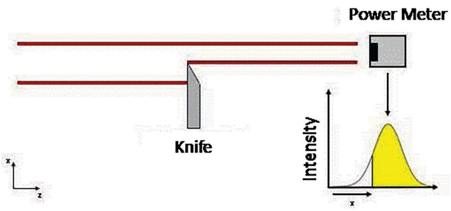

Figure 4: Knife-Edge method.

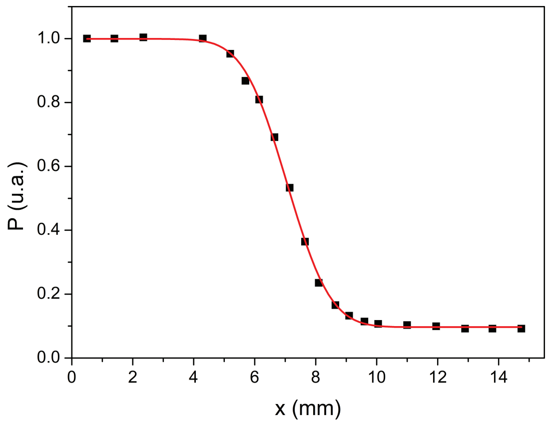

Figure 5: Knife-edge method performed at a distance of 183 mm from Lens $f = 250$ mm. Measured waist $w = 2.22 \pm 0.06$ mm.

powers for a given knife position. As x increases, the beam is blocked by the knife. In this measurement, the beam was cut at a distance of 183 mm from Lens $F3 = 250$ mm (Fig. 2). The red line represents the fit made by equation 10. The measured waist was $w(z = 183\ \text{mm}) = 2.22 \pm 0.06$ mm. In this measurement, the laser power was normalized, and a small residual power (P_{offset}) remained on the meter even when the beam was completely blocked due to an offset.

3.3. Smartphone camera method (SCM)

The alternative method for measuring w using a Smartphone camera was developed as follows: First, a thermochromic liquid crystal sheet (purchased on the website www.adesivisicurezza.it, *cost of* 12.25€) was positioned at the respective distances from Lens F3 where the knife had been placed. When the laser hit the sheet, it generated a color pattern in response to the temperature variation, which was recorded by a Samsung Galaxy S23 Smartphone camera positioned behind the sheet. For a laser exposure time of approximately 500 ms, we observed a pattern that evolved as shown in Figure 6. The laser exposure time was precisely controlled by a TTL pulse generated by a function generator coupled to the laser control box. This figure displays some frames from the recording ranging from a) 0 b) 1.5 s c) 3.2 s d) 5.0 s e) 7.4 s, and f) 9.5 s from the laser turns off. According to this figure we observe a recovery time of approximately 10 s before we can perform the next measurement. For each position of the sheet, the laser was triggered at least 10 times at 10 s intervals during a single recording. A millimeter scale was placed just above the pattern to calibrate the pixels during the analyses.

Next, we created a standardized analysis method. Firstly, we chose a frame that could provide consistent w values compared to those obtained by the knife-edge method. The selected frame was the one shown in Fig. 6(b) i.e. the 1.5 s frame. We chose this frame

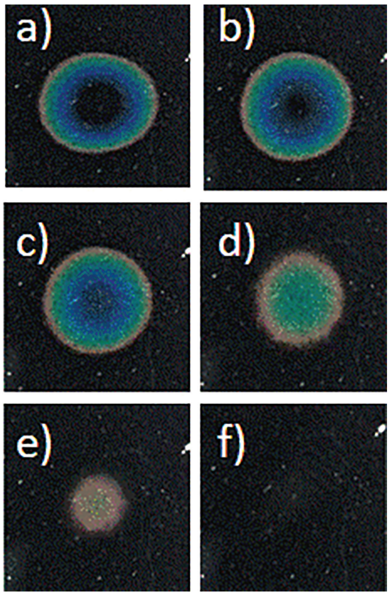

Figure 6: Evolution of the color pattern on the thermochromic sheet when the laser was exposed for 500 ms. Pattern recorded by a Smartphone camera. Figures (a) to (f) correspond to the following frames: (a) 0, (b) 1.5 s, (c) 3.2 s, (d) 5.0 s, (e) 7.4 s, and (f) 9.5 s.

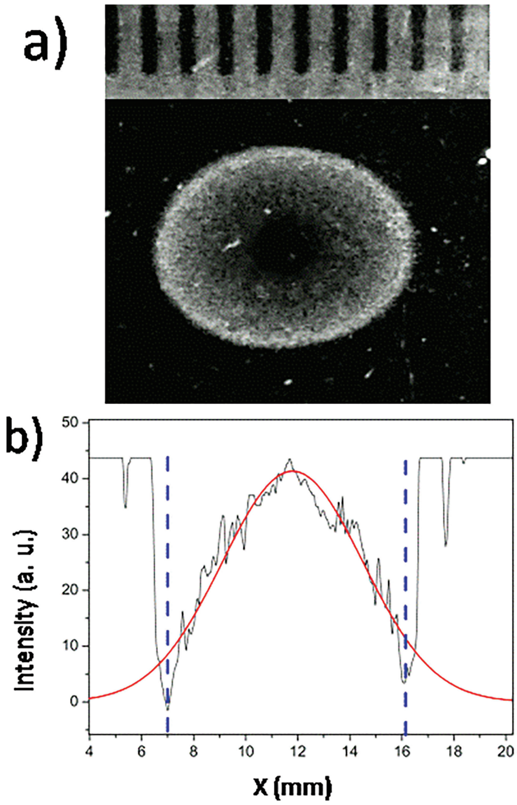

Figure 7: (a) Selected frame treated with specific brightness, contrast, and saturation adjustments. (b) Pixel intensity as a function of position (black line). The red line represents the Gaussian fit. The blue dashed lines delimit the region used for the fit. In this example, a $w = 4.2$ mm was calculated.

because it had a shape closer to a Gaussian distribution compared to the other frames. In the selected frame, we applied specific brightness, contrast, and saturation adjustments to obtain an image pattern like that in Figure 7(a). After the adjustment, the images were digitized to form a matrix where the rows and columns of the matrices represented positions (pixels), and their values were their intensity, which we directly correlated with radiation intensity. The color scale ranged from 0 for darker regions to 50000 for brighter regions. Using the central line of the matrix, specifically the line passing through the pattern's center, we obtained the shape of the black line in Fig. 7(b). To obtain this pattern, we inverted the colors by multiplying the pixel intensities by -1 and subtracting the offset. To calculate the $w(z)$, we fitted the data with the Gaussian function $I(x) = \frac{I_0^2 w_0^2}{w^2(z)} e^{-2(x-x_c)^2/w^2(z)}$ within the region delimited by the blue dashed line. The red line corresponds to this fit. Furthermore, in Fig. 7(b), it can be noticed that the measured pattern does not have an exactly Gaussian shape. However, this is expected since the pattern produced on the sheet is related to thermal effects that respond to both the laser intensity and the temperature of nearby surroundings.

4. Results

We applied the knife-edge method to a beam focused by a convergent lens with a focal length of 250 mm. The beam hit the lens's surface with an initial w of approximately 8.6 mm. Thus, we were able to produce various waists due to the longitudinal profile created by the lens. The beam was cut at six different positions as shown in column 1 of Table 1. Four cuts were made before the focus, and two cuts were made after the focus. In column 2 of Table 1, we have the waists calculated by the KEM. The smallest value obtained was $w = 220$ μm, which is closer to the lens's focus position. It is essential to note that the KEM starts losing precision near the focus region due to the challenges in positioning the knife accurately.

In column 2 of Table 1, we have the results of the waists calculated by the SCM. The average w value was obtained by applying the procedure described in section 3.3 to 10 different images while maintaining the same exposure time ($\sim$ 500 ms) and laser power ($\sim$ 1 W). The measurement error was calculated as the average deviation. The waists calculated at positions 61, 122, 305, and 366 mm were consistent with the KEM considering the error margin calculated by the SCM. The relative error between the methods starts to increase as the beam waist begins to decrease. In the case of the measurement taken near the focus, there is a relative error of 263%, indicating that the method is not suitable for measuring waists on the order of several hundred μm. The main reason is that the increased beam intensity

 DOI: https://doi.org/10.1590/1806-9126-RBEF-2023-0370

Table 1: $w(z)$ values obtained by both methods. For SCM we used the 1.5 s frame for all measurements.

z (mm) $\pm$ 0.5	w (mm) – KEM	w (mm) – SCM	Rel. error (%)
61	6.50 ± 0.20	6.3 ± 0.4	4
122	4.70 ± 0.20	4.4 ± 0.3	7
183	2.22 ± 0.09	2.9 ± 0.2	30
244	0.22 ± 0.04	0.8 ± 0.2	263
305	1.64 ± 0.07	1.9 ± 0.3	15
366	4.10 ± 0.10	4.1 ± 0.1	0

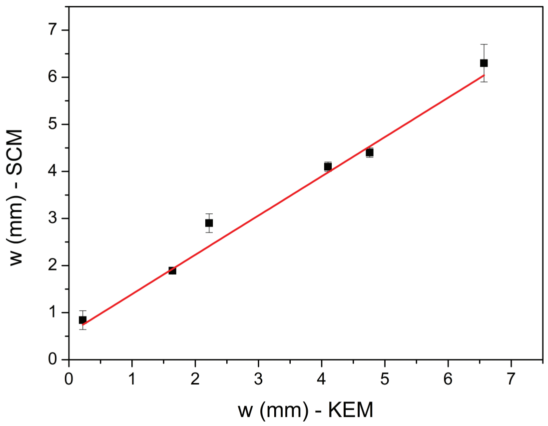

Figure 8: Comparison of the waists obtained by both methods. The red line represents a linear fit with a linear coefficient of 0.5 ± 0.1 and an angular coefficient of 0.83 ± 0.04.

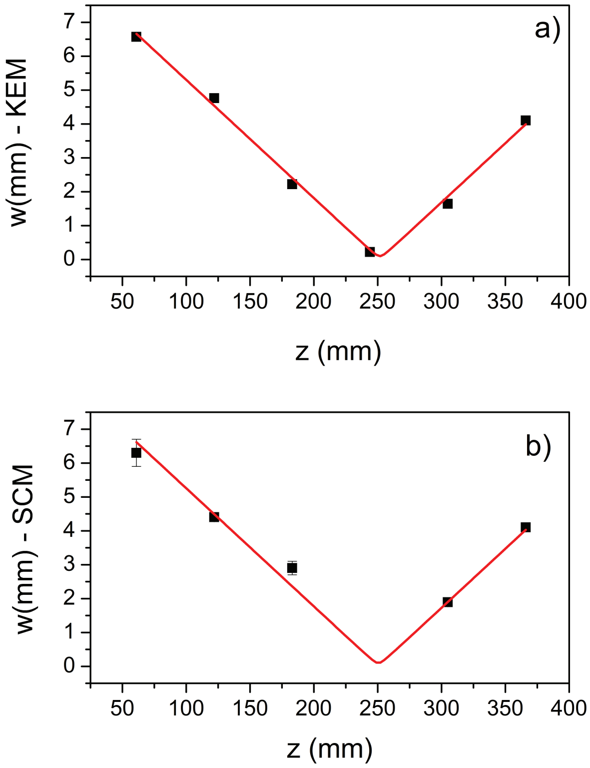

Figure 9: Longitudinal profile of the beam created by a 250 mm lens. (a) Profile determined by KEM. (b) Profile determined by SCM. Both methods calculated $w_0 = 96 \pm 2$ μm and $z_c = 252 \pm 2$ mm.

near the focus causes the thermochromic sheet to burn, creating irreversible damage.

Figure 8 shows a comparison of the waists obtained by the SCM vs. KEM. A linear relationship can be observed between the two techniques. The red line corresponds to a linear fit with a linear coefficient of 0.5 ± 0.1 and an angular coefficient of 0.83 ± 0.04.

Although the SCM diverges for waists near the focus, it is possible to use these points to determine the value of the focus waist (w_0) and the focus position (z_c). For this calculation, we adjusted the points in Table 1 using the equation for the longitudinal profile of a Gaussian beam Eq. (8). Figures 9(a) and (b) show, respectively, the waists measured by the KEM and SCM as a function of distance. The red line represents the fit of the points by Eq. (8). The values obtained for the beam waist and focus position in both fits, considering significant number, were exactly the same: $w_0 = 96 \pm 2$ μm and $z_c = 252 \pm 2$ mm. It is important to note that in the analysis of the beam profile by the SCM, we excluded the point with the highest relative error, which is the point measured at $z = 244$ mm. For comparison, the theoretical value of the focus power of a lens for a Gaussian beam can be estimated using Eq. (11):

$$w_0 \approx \frac{2\lambda f}{\pi D} \tag{11}$$

where λ is the wavelength (10.6 μm), f is the lens's focal length (250 mm), and D is the beam diameter at the lens ($D = 2w_{Lens}$, approximately 17.8 mm). The estimated value for w_0 was 94.8 μm, which is consistent with the values obtained by both techniques. The M^2 factor, also called beam quality factor or beam propagation factor, is a common measure of the beam quality of a laser beam. M^2 factor can be defined as Eq. (12):

$$\theta = M^2 \frac{\lambda}{\pi w_0} \tag{12}$$

where θ is the half-angle beam divergence which can be calculated as the derivative of the beam radius with respect to the axial position in the far field, i.e., at a distance from the beam waist which is much larger than the Rayleigh length. For a single mode TEM_{00} (Gaussian) laser beam, M^2 is exactly one. In our experiment we calculate θ from the average of the slope module (from both sides of the focal region) of the red line in Figure 9. We obtained $\theta = 36$ mrad and a $M^2 = 1.023$ from both techniques.

5. Conclusion

Based on the results obtained using the knife-edge (KEM) and Smartphone camera (SCM) methods, we were able to analyze the behavior of Gaussian beam waists in relation to the lens's focal distance. The measurements showed good agreement between the two methods, especially at distances not too close to the lens's focus. However, we observed that the MCS tends to diverge when measuring waists near the focus, mainly due to the increased beam intensity. By comparing the results obtained by both methods, we established a linear relationship between the waists measured by the SCM and KEM. Furthermore, despite obtaining divergent w values near the focus region, it was still possible to use the SCM to estimate consistent values for the beam waist at the focus (w_0) and the focus position (z_c). These values were consistent with those obtained by conventional methods, reinforcing the validity of the SCM for determining Gaussian beam characteristics. In summary, our experiments demonstrated that the SCM can be applied under certain conditions for characterizing a Gaussian beam, providing consistent results compared to the KEM. This method could be a low-cost alternative for various applications in optics, lasers, and other fields related to light propagation involving the characterization of Gaussian beam longitudinal profiles.

Acknowledgements

This study was financed by Fundação de Amparo à Pesquisa do Estado de São Paulo (FAPESP), Grant number 2017/19248-3; Fundação de Amparo à Pesquisa de Minas Gerais – FAPEMIG (Grant number: APQ-00057-18).

References

[1] T.H. Maiman, Nature **187**, 493 (1960).
[2] J. Hecht, Opt. Eng. **49**, 091002 (2010).
[3] J.L. Bromberg, Phys. Today **41**, 26 (1988).
[4] A. Einstein, Erhandlungen der Dtsch. Phys. Gesellschaft **18**, 318 (1916).
[5] P.B. Bisht, *An Introduction to Photonics and Laser Physics with Applications* (IOP Publishing, Bristol, 2022).
[6] W. Demtröder, *Laser spectroscopy 1: basic principles* (Springer, Berlin, 2014).
[7] O. Svelto and D.C. Hanna, *Principles of lasers* (Springer, New York, 2010).
[8] Y.I. Khanin, *Fundamentals of laser dynamics* (Cambridge Int Science Publishing, Cambridge, 2006).
[9] R.E. Slusher, Rev. Mod. Phys. **71**, S471 (1999).
[10] T.W. Hänsch and H. Walther, Rev. Mod. Phys. **71**, S242 (1999).
[11] G.F. Borges, R.D. Baldijaõ, J.G.L. Condé, J.S. Cabral, B. Marques, M.T. Cunha, A. Cabello and S. Pádua, Phys. Rev. A **97**, 022301 (2018).
[12] J. Gea-Banacloche, Phys. Rev. A **65**, 22308 (2002).
[13] A. Kavokin, T.C.H. Liew, C. Schneider, P.G. Lagoudakis, S. Klembt and S. Hoefling, Nat. Rev. Phys. **4**, 435 (2022).
[14] B.S. Marangoni, C.R. Menegatti and L.G. Marcassa, J. Phys. B At. Mol. Opt. Phys. **45**, 175301 (2012).
[15] C.R. Menegatti, B.S. Marangoni and L.G. Marcassa, Phys. Rev. A **84**, 53405 (2011).
[16] J.S. Cabral, J.M. Kondo, L.F. Gonçalves, V.A. Nascimento, L.G. Marcassa, D. Booth, J. Tallant, A. Schwettmann, K.R. Overstreet, J. Sedlacek *et al.*, J. Phys. B At. Mol. Opt. Phys. **44**, 184007 (2011).
[17] T. Steinmetz, T. Wilken, C. Araujo-Hauck, R. Holzwarth, T.W. Hänsch, L. Pasquini, A. Manescau, S. D'Odorico, M.T. Murphy, T. Kentischer *et al.*, Science **321**, 1335 (2008).
[18] J.B. Bayle, B. Bonga, C. Caprini, D. Doneva, M. Muratore, A. Petiteau, E. Rossi and L. Shao, Nat. Astron. **6**, 1334 (2022).
[19] P. Polimeno, A. Magazzù, M.A. Iatì, F. Patti, R. Saija, C.D.E. Boschi, M.G. Donato, P.G. Gucciardi, P.H. Jones, G. Volpe *et al.*, J. Quant. Spectrosc. Radiat. Transf. **218**, 131 (2018).
[20] H. Moseley and V. Oswal, in: *Principles and Practice of Lasers in Otorhinolaryngology and Head and Neck Surgery*, edited by V. Oswal and M. Remacle (Kugler, Hague, 2002).
[21] G.N. Makarov, Physics-Uspekhi **56**, 643 (2013).
[22] Z. Ye, M. Su, J. Li, C. Jing, S. Xu, L. Liu, G. Ren and X. Wang, Opt. Laser Technol. **139**, 106988 (2021).
[23] W. Demtröder, *Laser spectroscopy* (Springer, Berlin, 1982).
[24] J.S. Cabral, C.R. Menegatti and G. Nicolodelli, Trends Anal. Chem. **160**, 116948 (2023).
[25] G. Nicolodelli, J. Cabral, C.R. Menegatti, B. Marangoni and G.S. Senesi, TrAC Trends Anal. Chem. **115**, 70 (2019).
[26] G.S. Senesi, J. Cabral, C.R. Menegatti, B. Marangoni and G. Nicolodelli, TrAC Trends Anal. Chem. **118**, 453 (2019).
[27] B.S. Marangoni, G. Nicolodelli, G.S. Senesi, N. Fonseca, H.J. Izario Filho, A.A. Xavier, P.R. Villas-Boas, D.M.B.P. Milori and C.R. Menegatti, Microchem. J. **165**, 106125 (2021).
[28] C.R. Menegatti, G. Nicolodelli, G.S. Senesi, O.A. Silva, H.J. Izario Filho, P.R. Villas-Boas, B.S. Marangoni and D.M.B.P. Milori, Appl. Phys. B **125**, 74 (2019).
[29] S. Genna, E. Menna, G. Rubino and V. Tagliaferri, Appl. Sci. **10**, (2020).
[30] A. Riveiro, F. Quintero, M. Boutinguiza, J. Del Val, R. Comesaña, F. Lusquiños and J. Pou, Materials (Basel) **12**, (2019).
[31] A. Farooq, A.B.S. Alquaity, M. Raza, E.F. Nasir, S. Yao and W. Ren, Prog. Energy Combust. Sci. **91**, 100997 (2022).
[32] J. Schlarp, E. Csencsics and G. Schitter, IEEE Trans. Instrum. Meas. **69**, 3606 (2020).
[33] J.M. Khosrofian and B.A. Garetz, Appl. Opt. **22**, 3406 (1983).
[34] W. Plass, R. Maestle, K. Wittig, A. Voss and A. Giesen, Opt. Commun. **134**, 21 (1997).